

Cloud Regimes and Cloud Types Associated With Squall Lines

Jo Yu Wu*

Department of Atmospheric Sciences, National Taiwan University, Taipei, Taiwan

ABSTRACT

In this study, the brightness temperature was used to define the relevant sub-regions of the squall line, and the composition of its cloud regimes and traditional cloud types was analyzed and discussed. It can be known that in the squall line region, as to weather states (WSs), WS1 is dominated; in terms of cloud types, deep convective clouds are dominated. Moreover, in the rear and front regions, it can be seen that the proportion of deep convection in the rear region is higher than the proportion of suppressed convection; on the contrary, in the front region, the proportion of the latter is higher; these may relate to the clouds dynamical processes and some weather systems accompanied, e.g., the supercells and the surface fronts.

1. Introduction

Due to the geographical location and complex terrain of Taiwan, we are often affected or invaded by the mesoscale convective systems (MCSs). These systems often cause heavy rainfall in a short time period, and sometimes even cause terrible disasters. Therefore, a better understanding of MCSs is vital to disaster prevention in Taiwan. In addition, my own research is also dedicated to this point.

Squall lines are one of the common MCSs in Taiwan. A squall line is defined as any line or narrow band of active thunderstorms (Glossary of Meteorology). Previous research have mentioned that squall lines are generally observed to last several hours. These two basic features sharply distinguish the squall line from the more commonly observed mode of precipitating cumulus convection in which rain showers are widely scattered and intermittent (Rotunno et al. (1998)). Therefore, based on these two characteristics, subsequent researches on squall lines have developed several methods to define a squall line ([Table 1](#)).

As we can see in [Table 1](#), most studies use radar reflectivity and the length-width ratio (LWR) of convection systems (CSs) to identify squall lines. Owing to the limitation of the resolution of satellite data itself, researchers usually use it to study larger-scale weather systems or perform climate statistics. Obviously, due to the insufficient time and spatial scale of squall lines, few studies on squall lines use satellite data as the main source of research data.

Based on the limitations of the resolution, unlike most squall line studies that focus on the structure, environment, and maintenance mechanism of the squall line, this study mainly discusses the cloud composition of the squall line itself and also the surrounding. By the analysis of the

cloud regimes and traditional cloud types of the squall line, first, I hoped that the instinctive cloud composition of each sub-region, (e.g., stratified precipitation, convection, rear and front region), in the squall line structure can be basically verified. Then, I hope to further explore whether these types of cloud compositions can be attributed to the corresponding cloud dynamical processes.

This study focuses on issues mentioned above. It begin by describing the data and cases used, the method to define sub-regions for this work and some background knowledge of *cloud regimes* and *cloud types* in Section 2. In Section 3, it show the results and give corresponding analysis and discussion, which will be divided into two parts, *weather state (WSs)* and the *cloud types*. Finally, there will be a short conclusion and future work in Section 4 and Section 5, respectively.

2. Data and Methodology

a. Data and Study Cases

The HXG, HGGWS and HGG datasets from International Satellite Cloud Climatology Project (ISCCP) were used in this study. Overview of these data is shown in [Table 2](#). The HXG dataset, one kind of *ISCCP data*, which are the primary data products produced by the ISCCP processing of satellite observations. Moreover, the HXG data saves the index of variables, which means the actual values need to be extracted from an *index table* for each variable. Instead, HGG data is a kind of *ISCCP basic data*, which is a subset of the variables from the complete ISCCP dataset that focuses on the most basic cloud parameters. Different from *ISCCP data*, the *ISCCP basic data*, namely HGG data, saves the true values of each variable. As to HGGWS dataset, it includes the variables of *ws* for the *mean PC-τ*

*Corresponding author: Jo Yu Wu, 861126iris@gmail.com

TABLE 2. Overview of ISCCP datasets in this study

	HXG	HGGWS	HGG
Spatial Resolution	$0.1^\circ * 0.1^\circ$	$1^\circ * 1^\circ$	$1^\circ * 1^\circ$
Temporal Resolution	3 hr intervals	3 hr intervals	3 hr intervals
Format	netCDF	netCDF	netCDF
Variables	itmp	ws	cldamt_types

TABLE 3. Brief information of squall line cases in this study

Case No.	Area	Time	Source of Info.
1	Taiwan	1997/11/26	Chen et al. (2007)
2	Taiwan	2006/05/02	Huang (2006)
3	China	2007/04/24	Zhou (2016)
4	China	2008/06/20	Meng et al. (2013)
5	the US	2012/03/20	NWS
6	Korea	2013/06/18	Kim et al. (2019)
7	China	2014/05/22	Qian et al. (2018)
8	the US	2017/02/19	Williams et al. (2019)
9	the US	2017/03/29	NWS
10	the US	2017/05/16	NWS

TABLE 1. Several of the criteria used to define squall lines in previous research. (Meng et al. (2013), Table 1)

	Chen and Chou (1993)	Chen and Chou (1998)	Parker and Johnson (2000)	Meng and Zhang (2012)	Meng et al. (2013)
Criteria					
(a) Band of larger than 12 dBZ $\geq 150\text{km}$ and lasting $\geq 5h$	(a) Band of larger than 20 dBZ $\geq 100\text{km}$ and lasting $\geq 4h$	(a) Band of contiguous or quasi-contiguous larger than 40 dBZ $\geq 100\text{km}$ and lasting $\geq 3h$	As in Parker and Johnson (2000); “quasi contiguous” was interpreted as that 40-dBZ band can be noncontiguous but the 35-dBZ band in which the 40-dBZ convection is embedded in has to be strictly contiguous	As in Parker and Johnson (2000), but here the 40-dBZ convection is strictly contiguous	
(b) LWR of larger than 36-dBZ band $\geq 3:1$ at mature	(b) Band of larger than 40 dBZ lasting $\geq 2h$ with an LWR $\geq 5:1$ common leading edge	(b) Linear or quasi-linear convective area sharing a common leading edge			

for whole global and also january, february, march, etc, which are the *weather states (WSs)* data for every 3 hr in each month. Note that the spatial resolution is $0.1^\circ * 0.1^\circ$, $1^\circ * 1^\circ$ and $1^\circ * 1^\circ$ for HXG, HGGWS and HGG datasets, respectively.

Because of the lack of reference previous researches using satellite data to define a squall line, and the concern of misjudgment, in this short project, I finally decided to use the squall line cases that mentioned in some previous researches or the NWS records, as shown in Table 3, for the following analysis steps.

b. Definition of sub-regions

To define the sub-regions for this study, first, I used brightness temperature (TB), *itmp* in HXG dataset. A threshold, $\text{TB} \leq 230\text{K}$, is applied and the minimum bounding rectangular (MBR), which includes all the points satisfied the threshold, roughly identifies the *squall line region* (Figure 1(b)). With the squall line region is determined, the area in same height with squall line region and extends, in the *opposite* direction of the storm motion, twice the width of the squall line region from the rear boundary of the squall line region is defined as the *rear region* (Figure 1(a)). Similarly, the area in same height with squall line region and extends, in the *same* direction of the storm motion, the width of the squall line region from the front boundary of the squall line region is defined as the *front region* (Figure 1(c)). The sub-regions, framed by a red rectangle and two black lines, for each case in this study is shown in Figure 2.

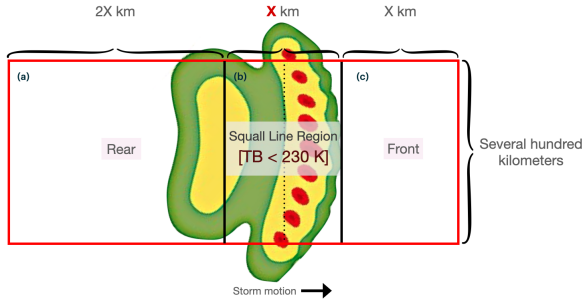


FIG. 1. Conceptual model of sub-regions in this study; (a) rear region, (b) squall line region and (c) front region

c. Cloud Regimes and Cloud Types

Based on their height and shape, clouds are traditionally classified into nine cloud types, including *deep convection* (*Dc*), *Cirrostratus* (*Cs*), *Cirrus* (*Ci*), *Nimbostratus* (*Ns*), *Altocstratus* (*As*), *Altocumulus* (*Ac*), *Stratus* (*St*), *Stratocumulus* (*Sc*) and *Cumulus* (*Cu*). However, Warren et al. (1985) mentioned that it is common for two or more cloud types to occur simultaneously, which means that if we considered only traditional cloud types, it may not be such representative and practical. Moreover, Rémillard and Tselioudis (2015) have mentioned that the cloud regimes analysis makes it possible to examine cloud interactions with atmospheric processes at a wide range of time and space scales; and it can be constructed either through the application of data analysis techniques directly on properties of the cloud field itself or through the derivation of regimes from analysis of dynamic and/or thermodynamic atmospheric parameters and the subsequent compositing of the corresponding cloud properties for each regime. In this study, I use the first method, Similar to the methods in some previous studies have applied (e.g., Jakob and Tselioudis (2003); Rossow et al. (2005); Tselioudis et al. (2013)). With applying this technique to the whole globe, we get 11 centroids (Figure 3), which is referred as the *weather states* (*WSs*) since it has been shown that the cloud property patterns thus detected are linked to distinct states of the atmosphere (Jakob and Tselioudis (2003); Jakob and Schumacher (2008); Tselioudis et al. (2013)). Furthermore, 11 WSs can be roughly classified into 3 WSs classes: WS1 to WS3 belong to *convective active* (*C*) class; WS4 to WS6 belong to *intermediate* (*I*) class; WS7 to WS10 belong to *convective suppressed* (*S*) class (Tan and Jakob (2013)), which will also be discussed in the next section.

3. Results and Discussion

a. Weather States (WSs)

1) 11 WSs

Applying the ISCCP HGGWS data to each case, we get the results shown in Figure 4. Besides, Figure 7(a)-(c)

show the composite kernel density estimation (KDE) of 11 WSs for all cases in each sub-regions.

As for the squall line region, in Figure 7(a), first, it is not surprising to find WS1 dominates the squall line region, because WS1 indicates the convective-active weather state (Figure 3), nearly represents the deep convection which is common in the convective band in a squall line system. Second, there is a minor peak at WS7. WS7 belongs to convective-suppressed weather state. One reason for this extreme value may be that triggered new cells have not yet developed to the extent of deep convection. Another reason may be caused by the evaporation cooling, entrainment effect or the rear-to-front (RTF) flow in mature squall lines, which produces downdraft to inhibit the development of convection beside the convective zone in a squall line. Still another reason may be the compensated sinking motion around a squall line system, which suppresses convection to grow. Besides, there is also a tiny peak at WS5 in Figure 7(a). In Figure 3, we can find that the altostratus and nimbostratus clouds account for the most. I think it may imply the stratiform precipitation.

As for the rear region (Figure 7(b)), we can find obvious maximums at WS2 and WS7. I think it is because the squall lines in several cases here are not isolated. Sometimes, squall line is a product of a supercell or a surface front. In this situation, the rear or even the front sub-regions may include some initial or even severe convective cells, which may increase the fraction of WS2 and WS7. Moreover, there is also a minor peak at WS5, as mentioned above, which may attribute to the stratiform precipitation.

As for the front region (Figure 7(c)), we can find obvious maximums at WS3 and WS7. In Figure 3, WS3 shows a high percentage in cirrus and altocumulus cloud, accompanied by some deep convective clouds. Notes that the fraction of WS7 is higher than that of WS3, which means the convective-suppressed is common in front region. Furthermore, there is also a minor peak at WS9. From Figure 3, we know that WS9, with a large proportion of cumulus and stratocumulus, belongs to convective-suppressed weather state. Thus, this situation may be caused by the similar reason as WS7 in squall line region.

2) 3 CLASSIFIED WSs

Similarly, using the classified WSs which are mentioned in Section 2, to replace the 11 WSs for each case, we will get the results shown in Figure 5. And, the composite fraction of 3 classified WSs for all cases in each sub-regions are shown in Figure 7(d)-(f).

Figure 7(d)-(f) show the similar signals with Figure 7(a)-(c). Obviously, convective-active WS dominates in squall line region. For all sub-regions, the intermediate WS is less common. And, the convective-suppressed WS is considerable in rear and front region. Furthermore, we should notice that the fraction of convective-suppressed WS in

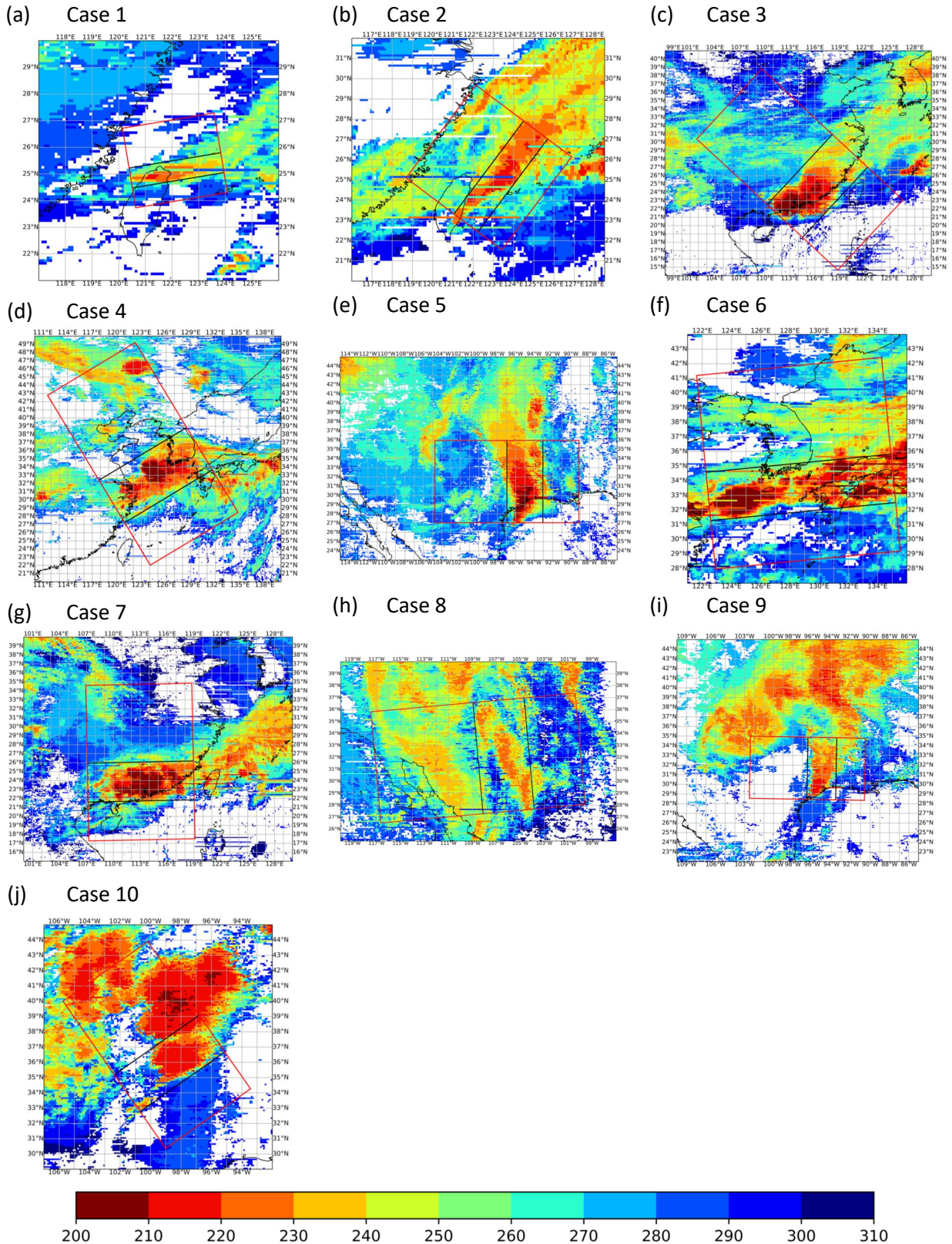


FIG. 2. Similar to Figure 1, but sub-regions for all cases in this study; shading represents the brightness temperature (TB; units: K)

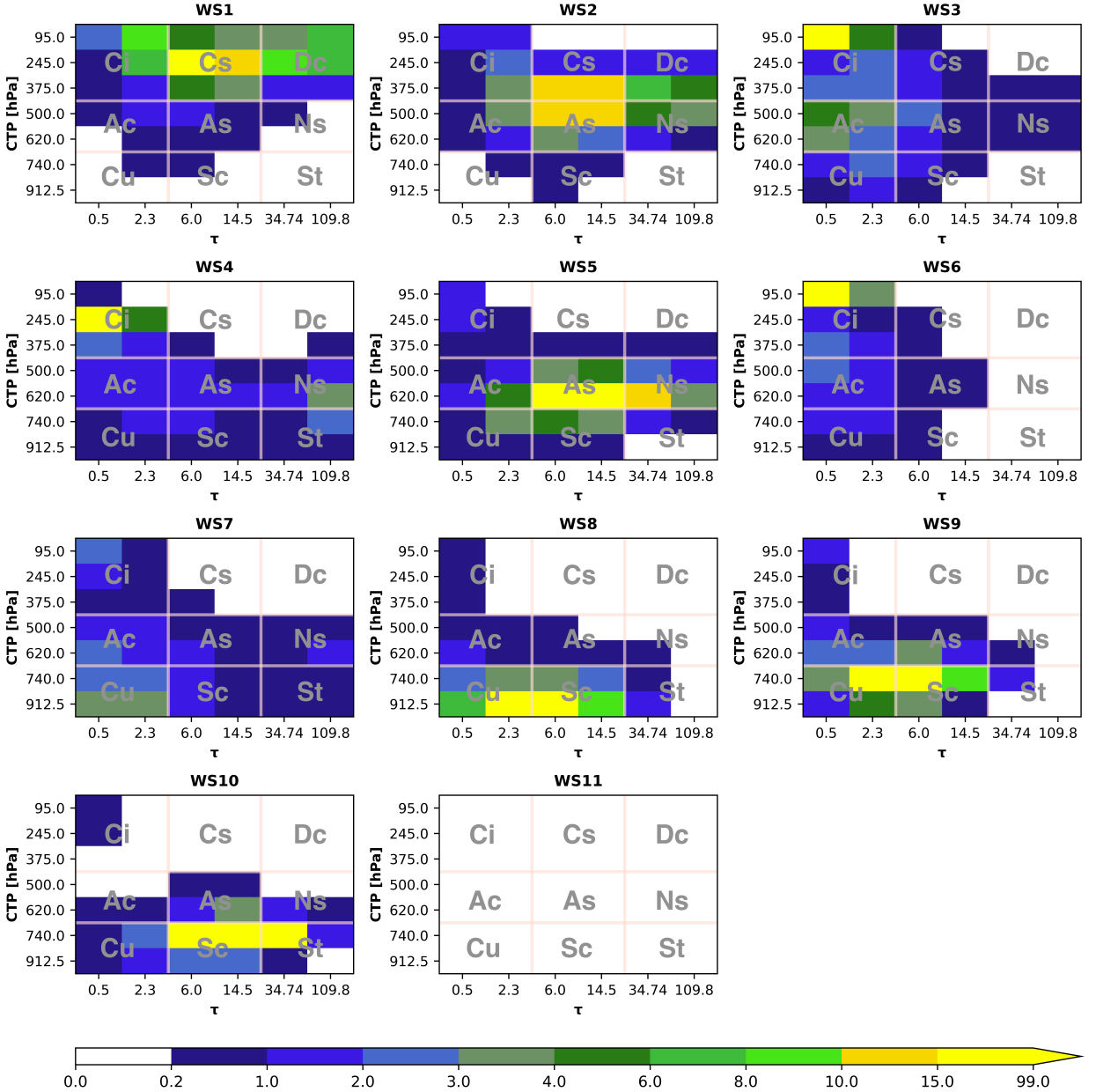


FIG. 3. 11 centroids of PC- τ plots for the global domain with nine cloud types symbols marked in each centroid

front region is more than that in rear region, and in contrast, the convective-active WS in rear region is more than that in front region. It is because, for the front region, where is the position the squall line moving on, it is reasonable that the developing convective cells will account for a large proportion, which may cause the higher percentage for convective-suppressed WS in the front region. On the contrary, with the possibility of the existence of accompanied systems, like some MCCs, supercell or surface

front, makes the higher percentage for convective-active WS in the rear region.

b. Cloud Types

In Figure 6, taking case 3 as an example, we use the *cloud types* data in HGG files instead, which separates the outcome into nine parts, namely, nine cloud types (Figure 6(b)). Do this process for all cases in this study, we can get a composite KDE of nine cloud types in each sub-regions for each case, as figures shown in Figure 7(g)-(i).

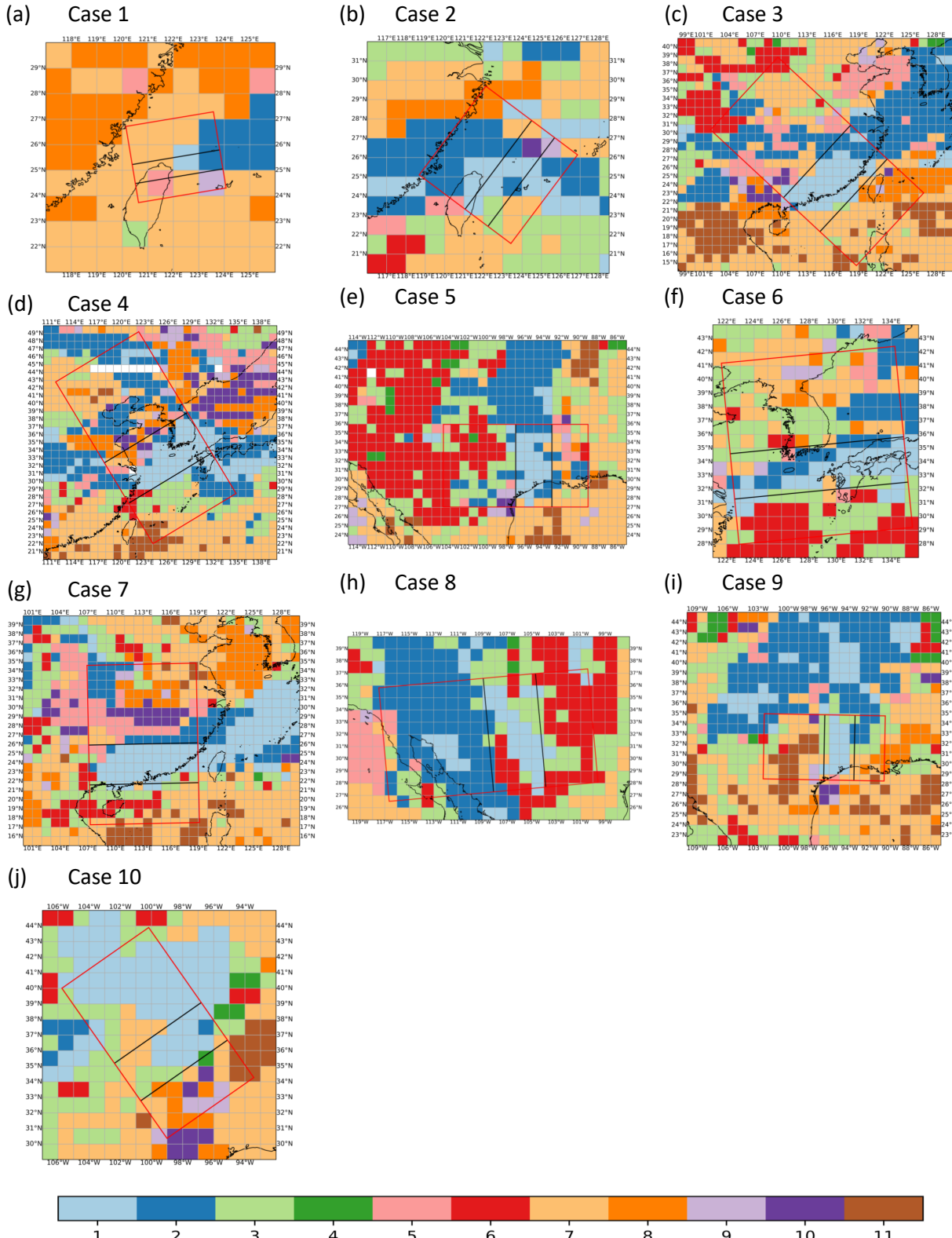


FIG. 4. Similar to Figure 2, but for WSs in shading

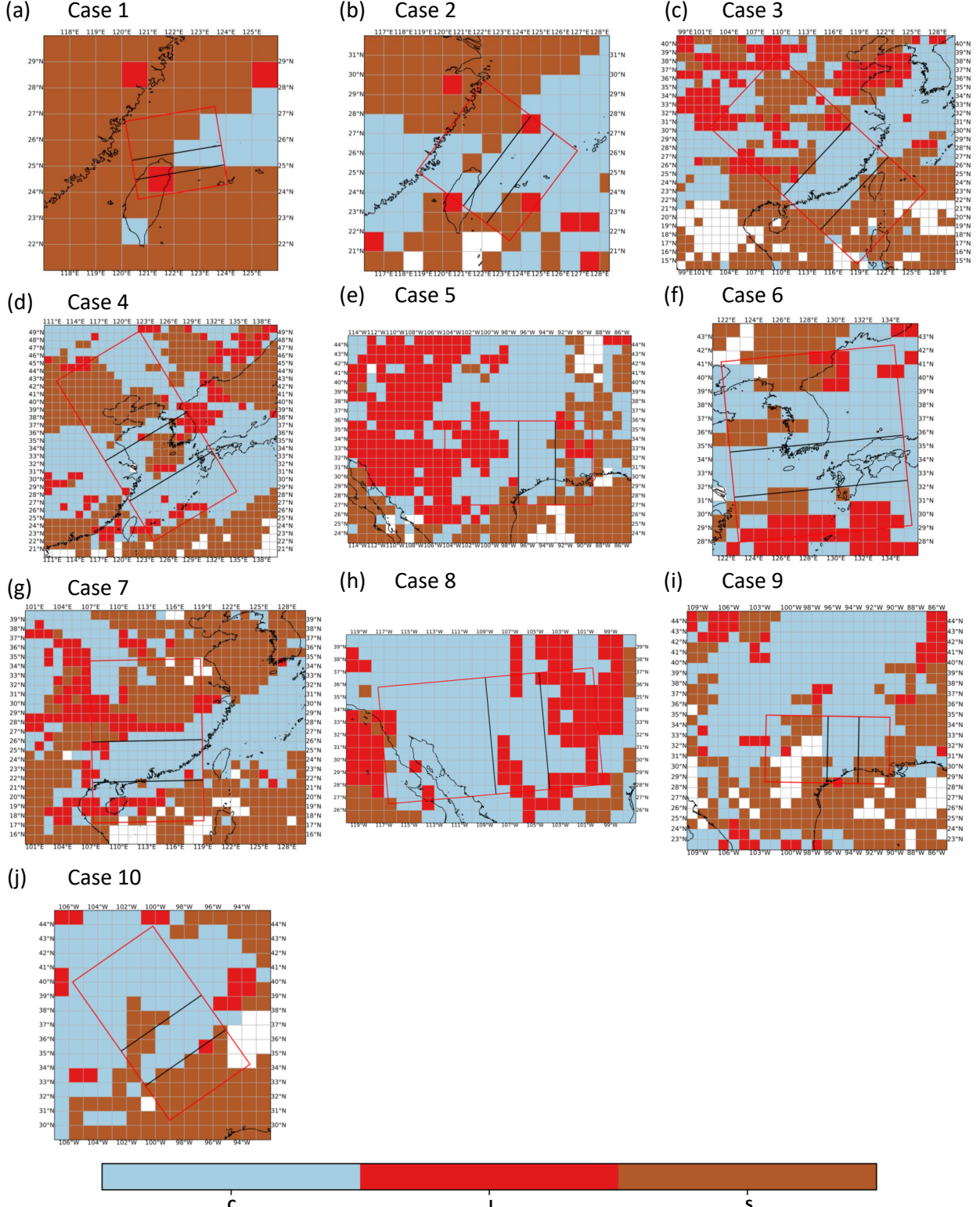


FIG. 5. Similar to Figure 1, but for 9 cloud types in shading in each plot. (C: Convective active; I: Intermediate; S: Convective suppressed)

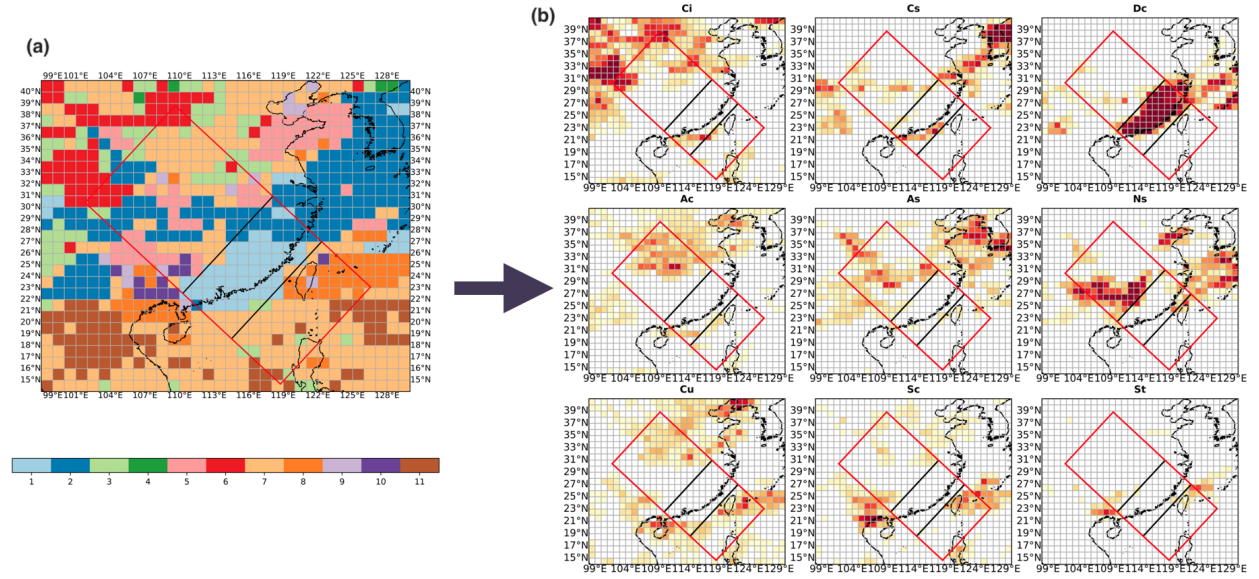


FIG. 6. (a) is same as Figure 4(c). (b) are the results of replacing the WSs with nine cloud types. The shading shows the percentage of occurrence for each cloud type; the darker the color, the higher the value

Again, the similar signal as Figure 7(a)-(c) appears in Figure 7(g)-(i). First, deep convection clouds dominates in squall line region. In rear region, the fraction of deep convection clouds is higher than that in front region. In contrast, the fraction of cumulus in front region is higher than that in rear region. Moreover, in Figure 7(h) and Figure 7(i), we can see that the rear and front region is similar in cloud types composition. The primary components of them all are cirrus, altostratus/altocumulus and stratocumulus/cumulus clouds. Note that the fraction of cirrus clouds in front region is the highest one among three sub-regions. However, I have not came up with a reasonable explanation for it yet, namely, it is still a unsolved issue so far; thus, it will later be discussed in the *Future Work Section*.

4. Conclusions

Recall the objectives of this project: hope that can basically verify the instinctive cloud composition of each sub-region in the squall line structure. Then, hope to further explore whether these types of cloud combinations can be attributed to the corresponding cloud dynamical processes.

In view of the former, this project can draw the following conclusions. First, whether it is cloud regimes or cloud types, what is consistent with the facts is that the squall line area is dominated by WS1 and deep convective clouds. Moreover, there are a certain proportion of stratiform clouds, namely, WS5 for cloud regimes, in the rear region. Finally, compared to the rear region, the front region has a higher proportion of convective-suppressed

WS, or in cloud types aspect, a higher proportion of cumulus. This is because the front region is the area that squall line will approach, and triggered new cells may have a certain proportion in the region. On the contrary, the rear region is the area where the squall line will be far away, and should not have a large proportion of suppressed convective clouds. In addition, because some cases used in this study have accompanied by weather systems, such as supercells, cold fronts, etc.; thus, in the rear region, it can be found a higher proportion of deep convective clouds, namely, the WS1.

As for the latter, this study found that the convective-suppressed WS, or cumulus, exists in all sub-regions may owing to the downdraft caused by evaporation cooling, entrainment effect or RTF flow, and also the compensated sinking motion around the squall lines; both of them may induce the development of convective-suppressed WS and inhibit the development of convective-active WS. Moreover, the result may have something to do with the triggered new cells.

5. Future Work

In this study, due to the lack of a specific method to define squall lines by satellite data, there are only ten cases considered. Thus, the conclusions drawn may not be so convincing and credible. As to the future work, first, using the reflectivity data of ground radars to determine and extract all MCSs that satisfy the criteria, which will be regard as a squall line case member. Then, define the sub-regions for all members and use satellite data to do the following analysis of their cloud regimes and cloud types.

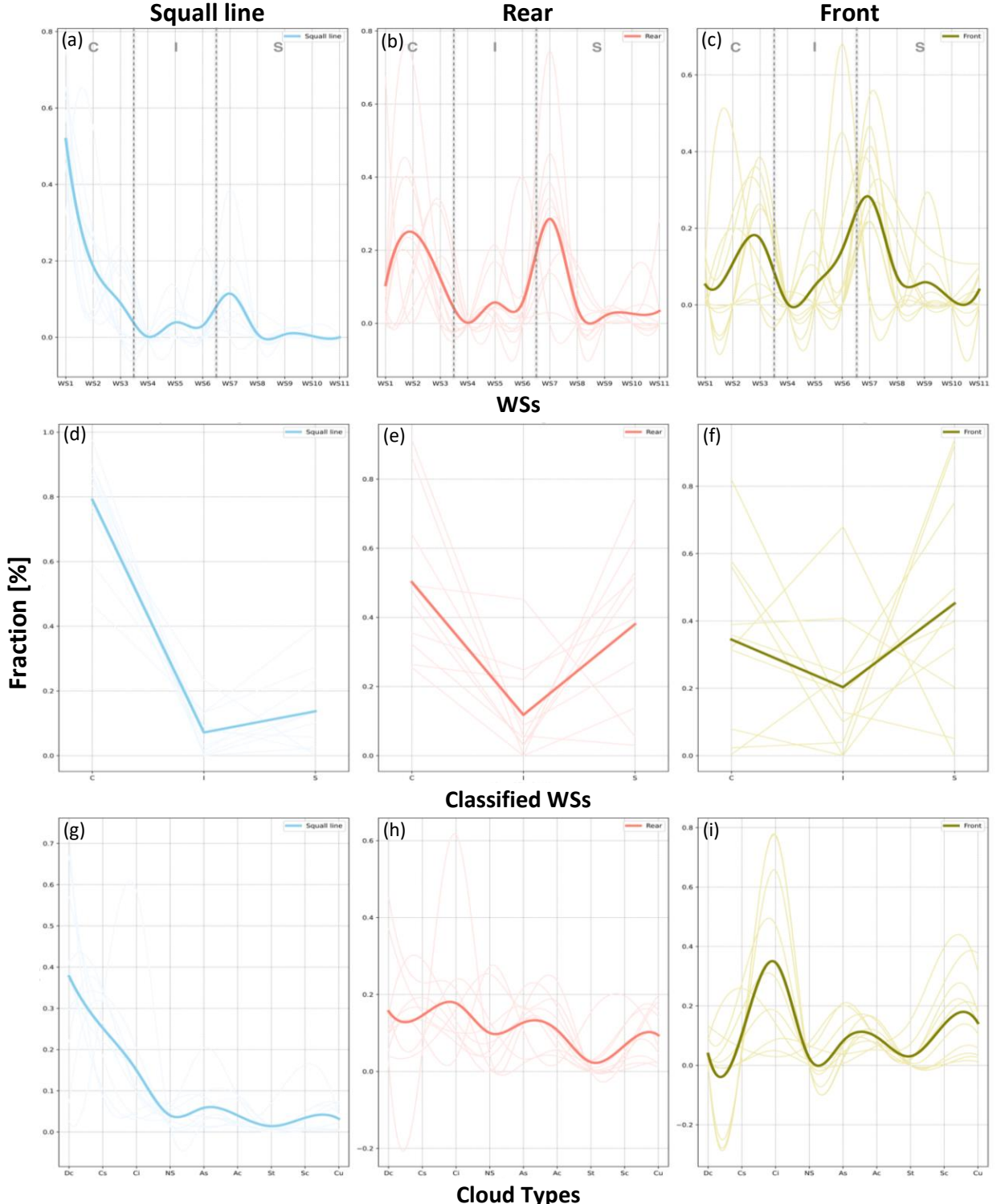


FIG. 7. (a)-(c) are the composite KDE of 11 WSs for squall line, rear and front sub-regions, respectively. (d)-(f) are similar to (a)-(c), but for 3 WSs classes. (g)-(i) are similar to (a)-(c), but for 9 cloud types. Note that the 3 classified WSs are marked in (a)-(c) by "C", "I" and "S", respectively, and separated by two gray dash lines. The dark thick line(light thin lines) in each plot represent the mean(the values) of all cases in this study

TABLE 4. Definitions of various radar traits of the squall lines in Meng and Zhang (2012).

Formation time	When the squall line threshold is first met
Dissipation time	Time when the squall-line threshold is continuously last met for more than 3 h after its formation
Duration	Period during which the squall-line threshold is continuously met
Max length	The length of the maximum straight long axis of a contiguous 40-dBZ reflectivity band
Orientation	The dominant orientation during the life span of a squall line using the azimuthal angle of a straight line connecting the two endpoints of the 40-dBZ band [similar to Parker and Johnson (2000)]
Speed of movement	The length of a straight line connecting the midpoints of the hourly isochrones at the leading edge of the quasi-linear 40-dBZ band during the lifetime divided by the lifetime (similar to Wyss and Emanuel 1988; Parker and Johnson 2000)
Intensity	The maximum value of the radar composite reflectivity during the lifetime
Formation mode	The dominant mode used to represent the formation process of a squall line, including broken line, back building, broken areal, and embedded areal, as defined by Bluestein and Jain (1985)
Organizational mode	The dominant juxtaposition of stratiform and convective rainfall, including leading stratiform, trailing stratiform, and parallel stratiform, as defined by Parker and Johnson (2000)

In addition, with the definitions to identified the life stage of a squall line in Meng and Zhang (2012) (Table 4), I am interesting in whether for the squall lines on different life stages, will I get the same results? Furthermore, as mentioned in the end of Section 3. I am wandering whether the cirrus really accounts for large percentage in the front region. It may also need the large number of case members to join to figure out whether the situation is indeed truth.

Acknowledgments. Thank Prof. Luo for giving some insightful comments, constructive suggestions and helping me a lots during the period of conducting this project.

References

- Chen, G. T.-J., and H.-C. Chou, 1993: General characteristics of squall lines observed in tamex. *Mon. Wea. Rev.*, **121**, 726–733.
- Chen, G. T.-J., and H.-C. Chou, 1998: Mesoscale convective systems in the southeast united states during 1994–95. A survey. *Wea. Forecasting*, **13**, 860–869.
- Chen, G. T.-J., C. C. Wang, and H.-C. Chou, 2007: Case study of a bow echo near taiwan during wintertime. *J. Meteorol. Soc. Japan*, **85**, 233–253.
- Huang, Y. N., 2006: A case study of a fast moving convective system observed on 1-2 may.
- Jakob, C., and C. Schumacher, 2008: Precipitation and latent heat- ing characteristics of the major tropical western pacific cloud regimes. *J. Climate*, **21**, 4348–4364, doi:10.1175/2008JCLI2122.1.
- Jakob, C., and G. Tselioudis, 2003: Objective identification of cloud regimes in the tropical western pacific. *Geophys. Res. Lett.*, **30**, 2082, doi:10.1029/2003GL018367.
- Kim, M. S., B. Campistron, and B. H. Kwon, 2019: Frontal wind field retrieval based on uhf wind profiler radars and s-band radars network. *Atmosphere 2019*, **10**, 547, doi:10.3390/atmos10090547, www.mdpi.com/journal/atmosphere.
- Meng, Z. Y., D. C. Yan, and Y. J. Zhang, 2013: Wind structure of a subtropical squall line in china: Results from dual-doppler radar data. *Mon. Wea. Rev.*, **141**, 1629–1647.
- Meng, Z. Y., and Y. J. Zhang, 2012: On the squall lines preceding landfalling tropical cyclones in china. *Mon. Wea. Rev.*, **140**, 445–470.
- Parker, M. D., and R. H. Johnson, 2000: Organizational modes of mid- latitude mesoscale convective systems. *Mon. Wea. Rev.*, **128**, 3413–3436.
- Qian, Q., Y. Lin, Y. Luo, X. Zhao, Z. Zhao, Y. Luo, and X. Liu, 2018: Sensitivity of a simulated squall line during southern china mon-soon rainfall experiment to parameterization of microphysics. *J. Geo- phys. Res. D.: Atmos.*, **123**, 4197–4220, doi:10.1002/2017JD027734, <https://doi.org/10.1002/2017JD027734>.
- Rossow, W. B., G. Tselioudis, A. Polak, and C. Jakob, 2005: Tropical climate described as a distribution of weather states indicated by distinct mesoscale cloud property mixtures. *Geophys. Res. Lett.*, **32**, L21 812, doi:10.1029/2005GL024584.
- Rotunno, R., J. B. Klemp, and M. L. Weisman, 1998: A theory for strong, long-lived squall lines. *J. Atmos. Sci.*, **45**, 463–485.
- Rémillard, J., and G. Tselioudis, 2015: Cloud regime variability over the azores and its application to climate model evaluation. *J. Climate*, **28**, 9707–9720.
- Tan, J., and C. Jakob, 2013: A three-hourly data set of the tropical convection based on cloud regimes. *Geophys. Res. Lett.*, **40**, 1415–1419, doi:10.1002/grl.50294.
- Tselioudis, G., Y. Z. W. Rossow, and D. Konsta, 2013: Global weather states and their properties from passive and active satel- lite cloud retrievals. *J. Climate*, **26**, 7734–7746, doi:10.1007/s00382-007-0232-2.
- Warren, S. G., C. J. HaHn, and J. London, 1985: Simultaneous occur- rence of different cloud types. *J. Appl. Meteorol.*, **24**, 658–667.
- Williams, B. M., J. S. Allen, and J. W. Zeitler, 2019: Anticipating qlcs tornadogenesis: The three-ingredient method during the 19-20 february 2017 south-central texas tornadic qlcs event.
- Zhou, H. G., 2016: Wind structure of a subtropical squall line in china: Results from dual-doppler radar data. *Advances in Meteo- rology*, **2016**, 18 pages, <https://doi.org/10.1155/2016/9059383>.